J Solid State Electrochem (2008) 12:953–959
DOI 10.1007/s10008-007-0451-9

ORIGINAL PAPER

Synthesis of Mo-cluster compound, $LiHoMo_3O_8$ by carbothermal reduction and its reactivity towards Li

B. Das · M. V. Reddy · G. V. Subba Rao · B. V. R. Chowdari

Received: 13 July 2007 / Revised: 21 September 2007 / Accepted: 12 October 2007 / Published online: 13 November 2007

Abstract The mixed oxide containing the triangular molybdenum clusters, $LiHoMo_3O_8$, is prepared from the component oxides by one-step carbothermal reduction reaction at 750 °C. It was characterized by powder X-ray diffraction (XRD), scanning electron microscopy (SEM), and high-resolution transmission electron microscopy (HRTEM) techniques. Electrochemical studies were carried out at 24 °C and at 50 °C by galvanostatic cycling (range 0.005–3.0 V vs Li, at 30 mA/g) and cyclic voltammetry (CV). The first-cycle charge capacities at 24 °C and 50 °C after deep discharge to 0.005 V are 180 and 315 (±5) mAh/g, respectively, corresponding to ~3.5 and ~6.0 moles of Li per mole of $LiHoMo_3O_8$. Cycling up to 70 cycles at 24 °C shows a gradual increase in the reversible capacity and finally reaches 290 (±5) mAh/g (~5.6 moles of Li). When cycled at 50 °C, the reversible capacity reaches 470 (±5) mAh/g (~9.1 moles of Li) at the 40th cycle. The coulombic efficiency ranged from 96 to 98% (30–70 cycles; 24 °C). The differential capacity–voltage curves and the CV data show that the average potentials for the discharge- and charge process occur at 1.0 V and 2.2 V, respectively. The observed ex-situ XRD and HRTEM data on the electrodes in the discharged/charged states have been interpreted and a plausible reaction mechanism is proposed.

Keywords $LiHoMo_3O_8$ · Carbothermal reduction · Electrochemical properties · Anodes

Contribution to ICMAT 2007, Symposium K: Nanostructured and bulk materials for electrochemical power sources, July 1-6, 2007, Singapore.

B. Das · M. V. Reddy · G. V. Subba Rao · B. V. R. Chowdari (✉)
Department of Physics, National University of Singapore, Singapore, Singapore 117542
e-mail: phychowd@nus.edu.sg

Introduction

The eminently successful and commercially available lithium ion batteries (LIBs) employ the metal oxide, $LiCoO_2$ as the cathode electrode and graphite as the anode electrode material. During the charge–discharge cycling, the Li ions intercalate–de- intercalate into the electrodes and thus contribute to the capacity [1]. To reduce the cost, improve the capacity and safety-in-operation, efforts are being made to find alternative electrode materials for LIBs. Research on anode materials is focused on two directions: Tin (Sn) metal or binary and ternary amorphous and crystalline Sn-oxides, which can form an alloy with Li ($Li_{4.4}Sn$) at $V <$ 0.5 V vs Li. The capacity here arises from the reversible alloying–de-alloying reaction [2, 3]. The second approach is to make use of the formation/decomposition of Li_2O by the redox reaction ("conversion reaction") under ambient temperature electrochemical conditions, pioneered by Tarascon's group in the year 2000 [4]: $CoO + 2Li \leftrightarrow Li_2O + Co$. In recent years, several binary and ternary transitional metal oxides have been examined for their Li recyclability making use of the conversion reactions employing micron-size and nano-size (<100 nm) particles [3–5].

Molybdenum (Mo) containing mixed oxides have received attention as possible negative electrodes for use in LIBs [3]. This is due to the ability of the above metal ion to exist in several oxidation states in oxides, ranging from 3+ to 6+ and reversibly reacting with Li. Further, the high density of Mo-oxides can give rise to higher volumetric energy density of the electrode compared to the graphite. The compounds of the type $Na_{0.23}MoO_3$ [6, 7], $Mn_{1-x}(V_{1-x}Mo_x)_2O_6$ (x=0 and 0.4) [8, 9] and solid solutions, SnO_2–MoO_2[10] have been investigated. Other Mo-containing oxides studied are $MnMoO_4$ [11], $CaMoO_4$ [12], $MMoO_4$, (M= Cu, Zn, Ni, Fe) [13], and recently MoO_2 [14] and $(VO)MoO_4$ [15].

$LiHoMo_3O_8$ is one example of a large number of isostructural hexagonal layer-type compounds in which the layers of Mo ions and (Li, Ho) ions, respectively,occupy the alternate O-ion layers perpendicular to the *c*-axis [16, 17]. The Mo is in 4+ oxidation state and is in an octahedral environment of oxide ions, whereas the Li- and Ho ions adopt a tetrahedral and octahedral O coordination, respectively. The Ho ion can be replaced by other rare earth (Ln= Sm→Lu), Y, Sc, Ga or In, to give rise to isostructural compounds [16, 17]. An unusual feature in all these compounds is the existence of triangular Mo_3 clusters in which the Mo—Mo distance is less than that of the Mo–Mo distance in Mo metal. As the two 4d-electrons of each Mo^{4+} ion are trapped in the Mo–Mo bonds, the Mo_3 cluster does not possess a net magnetic moment. Thus, $LiHoMo_3O_8$ can only exhibit paramagnetism due to Ho^{3+} ions and electronically insulating behavior, even though detailed physical properties are not reported in the literature. $LiHoMo_3O_8$ and others in the series are usually prepared by solid state reaction of the constituent oxides or mixed oxides in evacuated and sealed quartz tubes at ~700–800 °C [16, 17].

We succeeded in preparing $LiHoMo_3O_8$ by the carbothermal reaction at 750 °C and for the first time, the Li-storage and recyclability of the above Mo-cluster compound has been examined. Preliminary results are reported here.

Experimental

The compound, $LiHoMo_3O_8$ (~5 g) was prepared by carbothermal reduction method. Stoichiometric mixture of high purity Ho_2O_3 (1.61 g) (Acros), LiOH (0.204 g) (Merck), MoO_3 (3.674 g) (Alfa AESAR), and carbon (0.306 g) (Super P MMM), were mixed thoroughly in a mechanical grinder and then pressed into a pellet. It was placed in a carbon crucible and heated in a tube furnace (Carbolite, UK) at 750 °C for 8 h in a flowing Ar atmosphere. After cooling to ambient temperature, the pellet was ground to powder and stored in desiccator.

For crystallographic analysis, powder X-ray diffraction (XRD) patterns were collected using Philips X'PERT MPD diffractometer equipped with Cu K_α radiation. The unit cell lattice parameters were obtained by the least square fitting (LSQ) of the selected higher angle lines in the XRD pattern. Morphological studies were conducted using scanning electron microscopy (SEM) (JEOL JSM6700F). The high-resolution transmission electron microscopy (HRTEM) and selected area electron diffraction (SAED) were carried out using the JEOL JEM3010 instrument operating at 300 kV. For HRTEM, the powder was dispersed in ethanol and a drop of suspension was deposited on a holey carbon-coated Cu grid.

The composite electrodes for electrochemical studies were fabricated by using a mixture of active material ($LiHoMo_3O_8$), super P carbon (electronically conducting additive) and polymer binder (PVDF) dissolved in *N*-methyl pyrrolidinone (NMP) in the weight ratio 70:15:15. The electrode slurry was coated on to an etched Cu foil (used as the current collector) (15 μm thick, Alpha Industries Co., Japan). After drying in an oven at 100 °C, it was pressed between stainless steel rollers, cut into circular strips, and vacuum dried. Glass microfiber filter (GF/F) (Whatman Int. Ltd, Maidstone, England) was used as the separator and the electrolyte used was 1 M $LiPF_6$ in ethylene carbonate (EC) + diethyl carbonate (DEC) (1:1) (Merck). The Li-metal foil (Kyokuto Metal Co., Japan) was the counter electrode and coin cells (size 2016) were fabricated in a glove box filled with Ar gas (Mbraun, Germany). Other details of the cell fabrication were described in earlier publications [12, 18].

The mass of the active material in the fabricated electrode is ~4–5 mg and the electrode area is 2 cm^2. Cyclic voltammetry and galvanostatic cycling of the cells were conducted using a potentiostat system (Mac-pile II, Bio-logic, France) and Bitrode multiple battery tester (Model SCN, USA) at ambient temperature (24 °C). For studies at 50 °C, the cells were kept in an oven and equilibrated. For recording the ex-situ XRD patterns, the cells were discharged or charged to the selected voltages, allowed to equilibrate and then dismantled in the glove box to recover the electrodes. Ex-situ TEM studies were carried out with the electrode material scraped from the Cu foil in a glove box and the powder was dispersed in ethanol by ultrasonic miller and deposited on a holey carbon grid. Other details have been reported elsewhere [5].

Results and discussion

Structure and morphology

Barker et al. [19, 20] have employed the carbothermal reduction reaction to prepare MoO_2 and $LiMoO_2$ in which Mo is in 4+ and 3+ valence states, respectively. Accordingly, we prepared $LiHoMo_3O_8$ by the following reaction at 750 °C in an Ar atmosphere:

$$LiOH + 1/2Ho_2O_3 + 3\ MoO_3 + 3C \rightarrow LiHoMo_3O_8 + 3CO + 1/2H_2O\ .$$

The freshly formed MoO_2 by the reduction of MoO_3 by carbon, reacts with Li_2O and Ho_2O_3 to form the desired compound. Optimization of temperature and time of reaction is necessary to obtain the pure product.

The $LiHoMo_3O_8$ compound is black and well crystalline and the XRD pattern showed lines characteristic of the

hexagonal structure, with small amounts (<5%) of the impurity phases identified as MoO_2 and Mo_5O_{14}. The indexed XRD pattern of the composite bare electrode is shown in Fig. 1a. The compound $LiHoMo_3O_8$ belongs to hexagonal P3m1 space group with the LSQ-fitted lattice parameter values, a=5.776(2) Å and c=5.150 (2) Å. These are in good agreement with those reported for $LiHoMo_3O_8$ (a=5.771 Å; c=5.156 Å) in JCPDS card no. 32-0562. The SEM micrograph of the compound showed particle sizes of submicron range, with agglomerated morphology (figure not shown). The HRTEM lattice image and SAED pattern of $LiHoMo_3O_8$ are shown in Fig. 2a and b, respectively. The value of 5.12 (±0.02) Å and 2.58 (±0.02) Å for the d-spacing of the planes in the lattice images correspond to (001) and (002) Miller indices, respectively. The observed d-values match well with the intense lines in the XRD pattern. The bright spots in the SAED pattern indicate excellent crystallinity of the compound and the identified Miller indices correspond to (001), (101), and (002) as is clearly seen in Fig. 2b.

Galvanostatic cycling

Galvanostatic charge–discharge cycling profiles of $LiHoMo_3O_8$ are shown in Fig. 3a–d. The cycling was carried out at a current density of 30 mA/g, in the voltage window, 0.005–3.0 V vs Li up to 70 and 40 cycles at 24 °C and 50 °C, respectively. The cells showed an open circuit voltage (OCV) about ~2.9 V. The first-discharge curve (Li-insertion reaction) at 24 °C showed minor voltage plateaux at ~1.51 V and a large plateau at ~1.0 V. This is followed by a continuous decrease of the voltage up to the deep discharge limit, 0.005 V. The existence of plateaux is indicative of the two-phase region. As can be seen, the capacity up to the end of the ~1 V-plateau region is 120 mAh/g.

Based on the formula weight of $LiHoMo_3O_8$ and mass of the active material in the electrode, this value corresponds to the consumption of ~2.3 moles of Li per mole of $LiHoMo_3O_8$. The total first-discharge capacity is 275 mAh/g (~5.3 moles of Li). During the first-charge cycle (Li extraction), the voltage plateau regions at ~1.0, 1.4, 1.7, and 2.2 V are clearly seen. However, except for the 1.0- and 2.2-V voltage plateaux, the capacities associated with the 1.4- and 1.7-V plateau regions are small (≤20 mAh/g). The total first-charge capacity is 180 mAh/g corresponding to ~3.5 moles of Li. Thus, the irreversible capacity loss (ICL) during the first discharge–charge cycle is ~1.8 moles of Li.

During the 2–20 cycles, the charge and discharge profiles follow a similar pattern with the voltage plateau regions clearly reproduced as in the first cycle. However, the width of the 1-V plateaux region during discharge and charge operation decreases with an increase in the cycle number. The reversible capacities show an increasing trend from 180 mAh/g. In the range 25–70 cycles, there is a qualitative change in the profiles as shown in Fig. 3b. The plateau region at ~1 V in the discharge profiles and at ~2.2 V in the charge profiles are only noticeable and all other minor voltage plateaux are eliminated. The capacity vs cycle number plot (Fig. 4) shows that the reversible capacity increases and reaches 290(±5) mAh/g at the end of 70 cycles. This value corresponds to 5.6 moles of Li. Assuming that $1C$= 290 mAh/g, the current rate corresponds to ~0.1 C. The coulombic efficiency (η) reaches 96–98%.

Voltage vs capacity profiles of $LiHoMo_3O_8$ recorded at 50 °C up to 40 cycles are shown in Fig. 3c and d. The observed voltage plateaux during cycling are similar to those encountered at 24 °C in the range 1–10 cycles. As can be expected, due to higher Li ionic conductivity of the electrolyte and better electrode kinetics at 50 °C in comparison to those at 24 °C, larger first discharge and charge capacities and larger reversible capacities have been recorded. Thus, the first discharge capacity is 480 mAh/g (9.2 moles of Li per mole of $LiHoMo_3O_8$), whereas the first charge capacity is 315 mAh/g (6.03 moles of Li) leading to an ICL of 165 mAh/g, which is larger than the ICL measured at 24 °C. In general, the ICL in the case of oxide anodes is known to arise due to intrinsic nature of the materials, electrolyte decomposition followed by the formation of the solid electrolyte interphase (SEI) and the formation of a 'polymeric film' covering the nano-sized particles of metal or metal oxide composites under deep discharge conditions [3–5].

From the 11th cycle onwards, a qualitative change occurs in the profiles, similar to the ones at 24 °C, where the two-phase regions (small voltage plateauxes) are eliminated. From Fig. 4 it is clear that the reversible capacity continuously

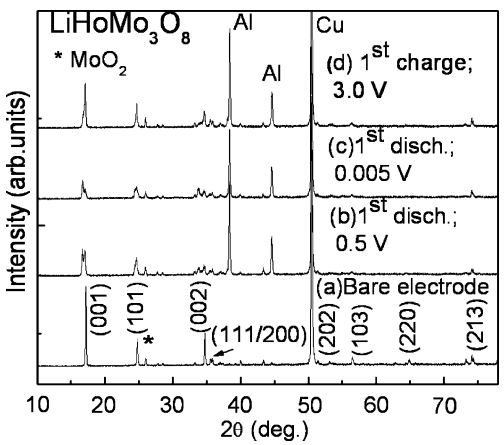

Fig. 1 X-ray diffraction patterns of $LiHoMo_3O_8$. **a** Bare electrode, **b** discharged to 0.5 V (vs Li), **c** discharged to 0.005 V, and **d** charged to 3.0 V during the first cycle. The Miller indices (h, k, l) are also shown. The lines due to Al, Cu metal and MoO_2 impurity are shown (Cu Kα radiation)

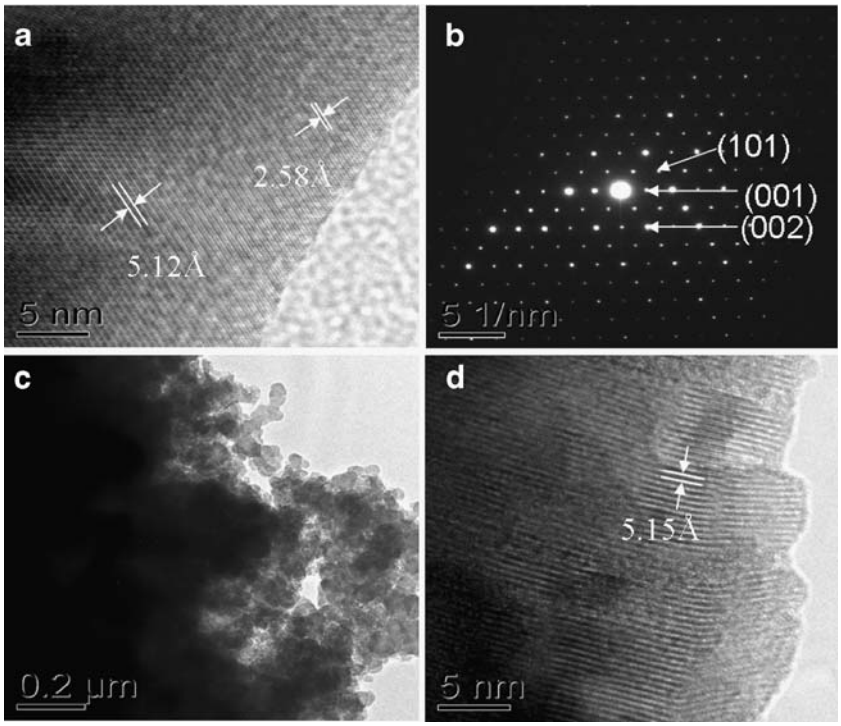

Fig. 2 **a** HRTEM lattice image and **b** the selected area electron diffraction (SAED) pattern of as-prepared $LiHoMo_3O_8$. **c**, **d** The TEM photograph and lattice image of the powder recovered from the cycled electrode (charged to 3.0 V after 70 cycles)

increases with the cycle number and reaches 470 (±5) mAh/g at the end of 40 cycles. This value corresponds to 9.1 moles of Li and almost matches with the first discharge capacity of 9.2 moles of Li. The current rate of 30 mA/g corresponds to ~0.06 *C* assuming that 1*C* = 470 mA/g. The coulombic efficiency (η) is 92–96% in the range of 12–40 cycles.

Cyclic voltammetry

Cyclic voltammograms (CV) were recorded on cells with $LiHoMo_3O_8$ as the active material at the slow scan rate of 58 μVs^{-1}, in the range 0.005–3.0 V at 24 °C, and are shown in Fig. 5a–b. The counter and reference electrode was Li metal. During the first cathodic scan minor peaks at

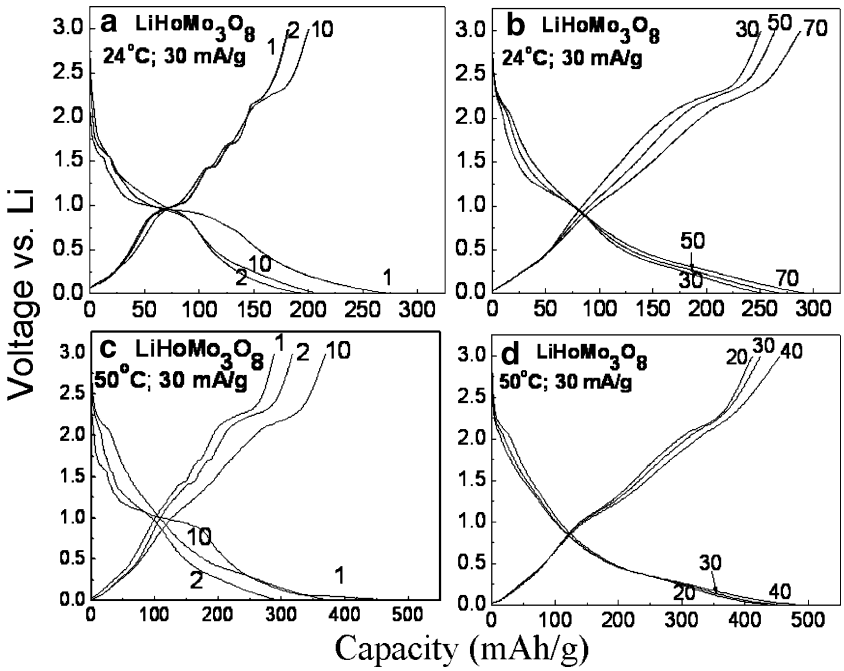

Fig. 3 Galvanostatic discharge–charge profiles (voltage vs capacity curves) of $LiHoMo_3O_8$ in the voltage range 0.005–3.0 V vs Li at a current of 30 mA/g. At 24 °C: **a** 1–10 cycles, **b** 30–70 cycles. At 50 °C: **c** 1–10 cycles, **d** 20–40 cycles. Only selected cycles are shown for clarity. The numbers indicate cycle number

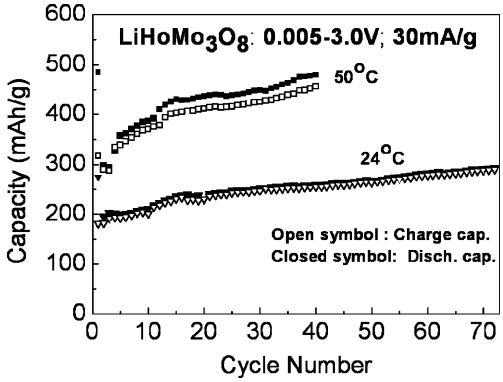

Fig. 4 Capacity vs cycle number plots of $LiHoMo_3O_8$ at 24 °C and 50 °C (voltage range, 0.005–3.0 V at 30 mA/g)

potentials 2.28, 1.72, and 1.51 V are seen, followed by the increase of current with an onset of peak at ~1.0 V and an intense peak at ~0.81 V. In the first-charge (anodic) curve, a split peak at ~1.0 V is seen, followed by peaks at 1.44, 1.71, and 2.2 V. The second cathodic sweep slightly differs from the first cathodic scan; the 2.28-V peak disappears and split peaks at ~1.6 V and a well-defined peak at ~0.90 V are clearly seen. The CVs remain essentially unchanged during the 10th, 20th, and 30th cycle (Fig. 5a,b). The peaks in the CV are an indication of two-phase reaction and/or phase transformation taking place in the material during cycling. The differential capacity (dQ/dV) vs voltage plots extracted from the voltage-capacity profiles of Fig. 3a,b are analogous to the CV profiles and these are shown in Fig. 5c,d. As can be seen, there is very good correspondence between the respective peak potentials in both the CV and (dQ/dV) vs V plots up to ten cycles. However, there is a marked difference in the (dQ/dV) vs V plots at the 20th and 30th cycles in that the anodic peaks below 2 V are very much reduced in intensity, whereas the intensity of the 2.2-V peak is increased. It is clear from Fig. 5d that the average discharge-voltage for Li-insertion is ~1.1 V, and the corresponding charge-voltage for Li-extraction is ~2.2 V.

Ex-situ XRD and TEM studies

It is well-known that the crystalline metal oxides like CoO [4], $ZnCo_2O_4$ [5], Na_xMoO_3 [6], and $CaMoO_4$ [12] are amorphised when electrochemically reacted with Li to the deep discharge limit (0.005 V vs Li), followed by reduction leading to the formation of Li_2O and metal nano-particles or a nano-composite "$M_xO_y - Li_2O$". The counter ions like Na or Ca act as 'matrices'. During the charge reaction, the Li is extracted from Li_2O or "$M_xO_y - Li_2O$" via the "conversion reaction." To clarify whether the crystalline $LiHoMo_3O_8$ is amorphised during the electrochemical Li insertion reaction, ex situ XRD patterns were taken after discharge to 0.5 and 0.005 V and also, after the first charge to 3.0 V. These are shown in Fig. 1, along with the XRD pattern of the virgin electrode.

The relative intensities (y axis) have been adjusted for easy comparison. The lines due to Al metal are from the sample holder and those from Cu metal are due to the current collector substrate. As can be seen in Fig. 1, the (001), (101), and (002) peaks in the XRD pattern of the bare electrode are split into doublet peaks in the patterns of the electrode recorded after the first discharge to 0.5 V (consumption of ~2.3 moles of Li; Fig. 3a) and 0.005 V (consumption of ~5.3 moles of Li). This can be interpreted as due to the coexistence of two phases, a Li-intercalated phase,

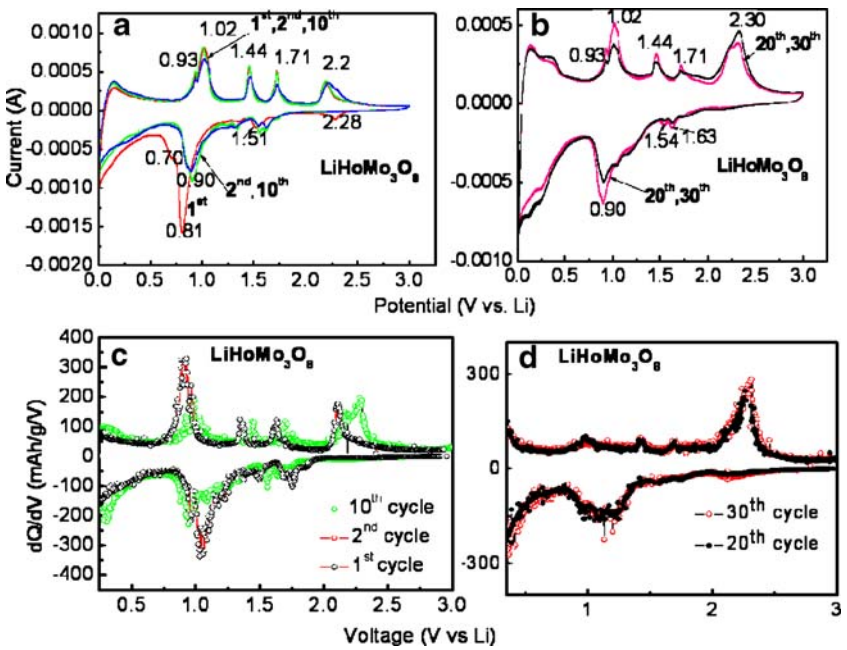

Fig. 5 Cyclic voltammograms of $LiHoMo_3O_8$ at the slow scan rate, 58 μVs^{-1} at 24 °C. **a** 1st, 2nd, and 10th cycles, **b** 20th and 30th cycles. Li metal was the reference and counter electrode. The numbers refer to the potential in volts. The differential capacity {dQ (mAh/g)/dV} vs voltage plots at 24 °C: **c** 1st, 2nd, and 10th cycles, and **d** 20th and 30th cycles. These were obtained from the voltage vs capacity profiles of Fig. 3a and b

$Li_{(1+x)}HoMo_3O_8$, with $x \leq 1$, and the host compound. From Fig. 1c, it is clear that the intensity of the (001) peak is smaller than that of the Li-intercalated phase.

The pattern recorded after the first charge (3.0 V) shows only the lines due to the host compound and those due to the Li-intercalated phase are practically absent (Fig. 1d). These observations show that, contrary to the expectations, the host crystal structure is not completely amorphised during the first discharge to 0.005 V vs Li. This is probably due to the highly electronically insulating nature of the compound, and Li is not able to penetrate completely in to the bulk of the submicron size particles. Figure 2c and d shows the HRTEM pattern and the lattice image, respectively, of the powder recovered after 70 discharge–charge cycles performed at 24 °C. There is evidence of some electrochemical pulverization of the particles (Fig. 2c), but the lattice spacing of 5.15 (±0.02) Å calculated from Fig. 2d matches well with the *d* value of the (001) line of the host compound, indicating some portion of the virgin compound is not at all affected after 70 cycles.

Reaction mechanism

Analogous to the reaction mechanisms established for the "conversion reactions" of metal oxides like CoO[4], $MnMoO_4$[11], or $CaMoO_4$[12] with Li, a plausible mechanism can be proposed based on the observed capacities and ex situ XRD data. When the cluster compound, $LiHoMo_3O_8$ is electrochemically discharged to 0.005 V vs Li metal, Li intercalation is possible due to the characteristic layer structure to give $Li_{(1+x)}HoMo_3O_8$, $x \leq 1$. Further reaction with Li will result in amorphisation and the formation of Li_2O, Ho_2O_3, and an X-ray amorphous "nano-composite" consisting of Mo-metal or "MoO_y" ($y < 2$) particles dispersed in a matrix of Li_2O, as per the Eq. 1. During the charge reaction (extraction of Li), the Mo metal particles can react with Li_2O by the displacement (conversion) reaction forming the respective nano-size metal oxides (Eq. 2). Thus, during the subsequent discharge–charge cycling, reversible reactions occur as per Eq. 2, and contribute to the capacity. Thus, we can expect a theoretical reversible capacity corresponding to 12 recyclable moles of Li per mole of $LiHoMo_3O_8$.

$$Li^{+}Ho^{3+}\left(Mo^{4+}\right)_3O_8 + 12\ Li \rightarrow 1/2Ho_2O_3 + 3Mo^{0}(\text{metal}) + (13/2)Li_2O \quad (1)$$

$$LiHoMo_3O_8 + 12Li \rightarrow 1/2Ho_2O_3 + 3'MoO_y' + (13-3y)/2)Li_2O \quad (1a)$$

$$3Mo + 6Li_2O \leftrightarrow 3M^{4+}O_2 + 12Li^{+} + 12e^{-}(\text{electrons}) \quad (2)$$

$$3'MoO_y' + 3xLi_2O \leftrightarrow 3MoO_2 + 6xLi^{+} + 6x\ e^{-}; (x+y) = 2 \quad (2a)$$

Reduction of Ho_2O_3 to Ho-metal by Li is not expected to occur under the ambient electrochemical conditions. It is possible that the formation of Mo^0 (metal) as per Eq. 1 may not occur always, and only an oxide, "MoO_y", with $0 < y < 2.0$, may form during the first discharge reaction (Eq. 1a). In fact, such a mechanism was proposed for $MnMoO_4$ [11], with $y = 1.0$. In that case, the expected theoretical reversible capacity will be $6x$ moles of Li ($x < 2$) per mole of $LiHoMo_3O_8$ (Eq. 2a).

The observed first discharge capacities correspond to 5.3 and 9.2 moles of Li per mole of $LiHoMo_3O_8$ when electrochemically reacted with Li at 24 °C and 50 °C, respectively. These values are lower than the expected consumption of 12 moles of Li as per Eq. 1. This indicates that all of the $LiHoMo_3O_8$ in the electrode has not reacted with Li due to the highly insulating nature (low electronic conductivity) of the compound. This conclusion is supported by the ex situ XRD of the discharged and charged electrodes and HRTEM of the charged electrode, which show the existence of crystalline $LiHoMo_3O_8$ in the fully discharged (to 0.005 V) and charged (to 3.0 V) electrode (Figs. 1 and 2c,d).

However, the first charge capacities of ~3.5 and ~6 moles of Li at 24 °C and 50 °C, respectively, do indicate that Li extraction is occurring from the "Ho_2O_3-Li_2O-Mo (or MoO_y)" composite, which has formed on the surface of the particles of the host material. The consistent increasing trend in the reversible capacity with the cycle number both at 24 °C and 50 °C (Fig. 4) does show that the "formation" or "formatting" of the electrode is not complete possibly due to kinetic reasons. Similar increase in capacity with the cycle number has been noticed by Guyomard et al. [21] in $LiMVO_4$ (*M* = Co, Ni, Zn, Cd) and recently, by the group of Tarascon [22], in nano-Fe_3O_4, even though the reasons are not yet clearly understood.

It is clear that the compound, $LiHoMo_3O_8$ is electrochemically active with regard to Li recycling and improvements in the capacity and cycling must be possible by improving its electronic conductivity, reduction of the particles to nano-size (<100 nm; e.g., by high-energy ball-milling) and/or surface modification (e.g., by coating with metal particles or conducting oxides). Work is underway along these lines.

Conclusions

The cluster compound with the hexagonal structure, $LiHoMo_3O_8$, has been prepared by one-step carbothermal

reduction method at 750 °C. It was characterized by XRD, SEM, HRTEM, and SAED, and its preliminary electrochemical cycling properties vs Li were studied. Galvanostatic charge–discharge cycling at current density 30 mA/g showed a gradual increase of reversible capacity in the voltage range 0.005–3.0 V with capacities of 290 and 470 (±5) mAh/g (corresponding to 5.6 and 9.1 moles of Li) at the *C* rates of 0.1 *C* and 0.06 *C* at the 70th and 40th cycle at 24 °C and 50 °C, respectively. The average charge potential and discharge potential are 2.2 V and 1.0 V, respectively. The coulombic efficiency ranges from 94 to 98%. The observed cyclic voltammograms have been interpreted in conjunction with differential capacity vs V plots. The ex-situ XRD and HRTEM data clearly showed that some portion of the virgin $LiHoMo_3O_8$ in the electrode remained unaffected by the Li cycling. A plausible mechanism for the Li insertion/extraction is proposed.

References

1. Van Schalkwijk WA, Scrosati B (eds) (2002) Advances in Lithium-Ion Batteries, Kluwer/Plenum, New York, USA
2. Courtney IA, McKinnon WR, Dahn JR (1999) J Electrochem Soc 146:59
3. Nazri G-A, Pistoia G (eds) (2003) Lithium Batteries: Science and Technology, Kluwer, New York, USA
4. Poizot P, Laruelle S, Grugeon S, Dupont L, Tarascon J-M (2000) Nature 407:496
5. Sharma Y, Sharma N, Subba Rao GV, Chowdari BVR (2007) Adv Fun Mater 17:2855
6. Leroux F, Goward GR, Power WP, Nazar LF (1998) Electrochem Solid State Lett 1:255
7. Leroux F, Nazar LF (2000) Solid State Ionics 133:37
8. Hara D, Ikuta H, Uchimoto Y, Wakihara M (2002) J Mater Chem 12:2507
9. Hara D, Shirakawa J, Ikuta H, Uchimoto Y, Wakihara M, Miyanaga T, Watanabe I (2003) J Mater Chem 13:897
10. Martos M, Morales J, Sanchez L (2002) J Mater Chem 12:2979
11. Kim SS, Ogura S, Ikuta H, Uchimoto Y, Wakihara M (2002) Solid State Ionics 146:249
12. Sharma N, Shaju KM, Subba Rao GV, Chowdari BVR, Dong ZL, White TJ (2004) Chem Mater 16:504
13. Leyzerovich NN, Bramnik KG, Buhrmester T, Ehrenberg H, Fuess H (2004) J Power Sources 127:76
14. Liang Y, Yang S, Yi Z, Lei X, Sun J, Zhou Y (2005) Mater Sci Eng B 121:152
15. Anji Reddy M, Satya Kishore M, Pralong V, Caignaert V, Varadaraju UV, Raveau B (2007) J Power Sources 168:509
16. Debenedittis J, Katz L (1965) Inorg Chem 4:1836
17. McCarroll WH (1977) Inorg Chem 16:3351
18. Reddy MV, Madhavi S, Subba Rao GV, Chowdari BVR (2006) J Power Sources 162:1312
19. Barker J, Saidi MY, Swoyer JL (2003) Solid State Ionics 158:261
20. Barker J, Saidi MY, Swoyer JL (2003) Electrochem and Solid-State Lett 6:A252
21. Guyomard D, Sigala C, Le Gal La Salle A, Piffard Y (1997) J Power Sources 68:692
22. Taberna PL, Mitra S, Poizot P, Simon P, Tarascon J-M (2006) Nat Mater 5:567